2019 SECED Conference
Earthquake risk and engineering towards a resilient world
9-10 September 2019, Greenwich, London

SEISMIC RESPONSE OF A R.C. STRUCTURE ISOLATED BY HDNR BEARINGS BY USING ADVANCED AND SIMPLIFIED MODELS

Laura RAGNI[1], Fabio MICOZZI[2], Enrico TUBALDI[3] & Andrea DALL'ASTA[4]

Abstract: *High Damping Natural Rubber (HDNR) bearings are characterized by stiffness and damping capacity that significantly depend on the shear deformation amplitude. Moreover, this type of bearings show a loading hysteresis dependence, due to the internal damage of the rubber occurring as the deformation history progresses. This effect, also known as stress-softening, becomes significant for large deformation amplitudes and leads to variability of the response, which has recently caused a limitation of the use of this type of isolators. However, the consequences of this nonlinear bearing behaviour on the response of isolated structures are not comprehensively investigated, primarily because advanced models have been developed only recently. In this paper, this issue is investigated by using a nonlinear constitutive law recently developed by some of the authors describing the behaviour of a HDNR with significant stress-softening complying with the limits of European code on anti-seismic devices. Numerical analyses are carried out on a multi-degree of freedom system by considering different seismic intensity levels and different response parameters, including floor response spectra. A linear visco-elastic model and an elastoplastic model, both calibrated at the third hysteresis cycle for each seismic intensity level, are also considered in the analyses for comparison. The obtained results show that some response amplifications happen due to the higher modes of the isolated structure, which are underestimated by the linear bearing model but well predicted by the elastoplastic one.*

Introduction

High Damping Natural Rubber (HDNR) bearings are widely used for seismic isolation because their low lateral stiffness and dissipating capacity. However, both stiffness and damping capacity strongly depend on the shear deformation amplitude. Moreover, in some rubber compounds the introduction of filler (added to increase the dissipation capacity) also induces a degradation of the cyclic response of the devices, due to an internal damage process occurring in the rubber. This effect, known as stress-softening or Mullins effect (Mullins 1969), characterizes the virgin rubber or a rubber that has recovered the original properties after a sufficient time of rest (Clark et al. 1997). The performance of structural and non-structural components of isolated system based on HDNR bearings at different intensity levels has been investigated in the past by using simplified models, such as linear viscoelastic models (Yang et al. 2010, Kelly and Marsico 2015) or elasto-plastic models (Isakovic et al. 2011). Thus, there is a need of more in-depth investigations on the potential effects of the nonlinear behaviour of HDNR bearings and this requires the use of models capable to describe these effects and their implementation within a finite-element framework. Some models Grant et al. 2004 and Kikuci et al. 2010) are currently available in the Opensees platform (McKenna et al. 2006) even if they show some approximations. Recently, an accurate nonlinear and history dependent constitutive law (Tubaldi et al. 2017 and Ragni et al. 2018) for describing the HDNR material behaviour with significant stress-softening but complying with the European code on anti-seismic devices (EN15129) has been developed. This model has been calibrated against the results of experimental tests carried out on several virgin rubber pieces and uses multiple damage parameters to simulate the stress-softening including its direction dependence.

In this paper, a multi-degree of freedom (M-DOF) system representing a realistic building with a hybrid isolation system consisting of HDNR bearings and low friction flat sliders is designed and analysed under serviceability and design conditions. In particular, the system is designed by following the European design codes (EN15129 and EN1998-1), i.e. by considering the seismic

[1] Associate Professor, Università Politecnica delle Marche, Ancona, Italy, laura.ragni@univpm.it
[2] PhD Student, University of Camerino, Ascoli Piceno, Italy, fabio.micozzi@unicam.it
[3] Lecturer, University of Strathclyde, Glasgow, UK; E-mail: enrico.tubaldi@strath.ac.uk
[4] Full Professor, University of Camerino, Ascoli Piceno, Italy, fabio.micozzi@unicam.it

action at the Ultimate Limit State (ULS), with return period T_R = 475 years. Nonlinear dynamic analyses are carried out under a set of real ground motion records scaled to different hazard levels, with return periods ranging from T_R = 30 years, typical of the Operational Limit State (OLS) of the Italian design code (NTC 2018) to T_R =475anni of the design limit state. The isolation system displacements and the superstructure inter-story drifts and absolute accelerations are evaluated. Moreover, floor response spectra are also derived to investigate the behaviour of rigid and flexible contents of the superstructure. In order to verify the effectiveness of simplified models in predicting the seismic response, analyses results are compared with those obtained by using a linear visco-elastic model as well as an elastoplastic model, both calibrated at the third hysteresis cycle and at each seismic intensity level, as suggested by the design code (EN15129).

HDNR behaviour

The HDNR compound adopted in this study exhibits a significant dissipation capacity, associated to a significant stress-softening. Nevertheless, the compound behaviour complies with the prescription of the European code on anti-seismic devices (EN15129) about the stability of the shear properties under repeated cycling, requiring a ratio between the minimum and the maximum shear modulus measured between the first and the tenth cycle of imposed harmonic strains not less than 0.6. The experimental characterization of the rubber are illustrated in detail in (Tubaldi et al. 2017 and Ragni et al. 2018), together with the calibration of the constative shear model (linking the shear stress τ_b to the shear strain γ_b) developed by some of the authors and able to simulate the hysteretic behaviour experimentally observed. Numerical hysteresis loops of virgin HDNR samples subjected each one to a maximum shear deformation ranging from 25% to 250% are reported in Figure 1. It can be observed that for low shear strain amplitudes (Figure 1a), the secant stiffness to maximum deformation decreases for increasing strain amplitudes and the stress-softening is limited. Differently, at large strain amplitudes, an hardening behaviour is observed and the stress-softening is more significant (Figure 1b). Cycles are carried out with a period equal to the isolation one. Nevertheless, this rubber compound shows a negligible dependence on the shear strain rate (Tubaldi et al. 2017). Figure 2 shows the equivalent linear proprieties of the HDNR compound for different strain amplitudes and loading cycles.

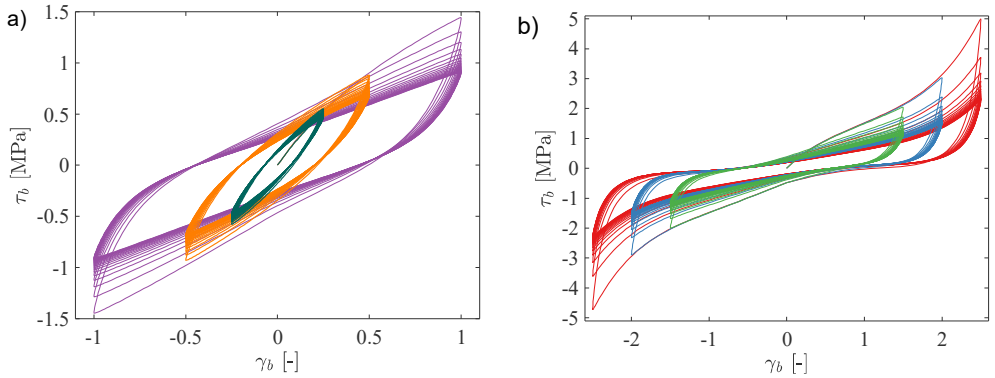

Figure 1: Hysteresis loops of virgin HDNR at different strain amplitudes: (a) 25%, 50% and 100% and (b) 150%, 200% and 250%.

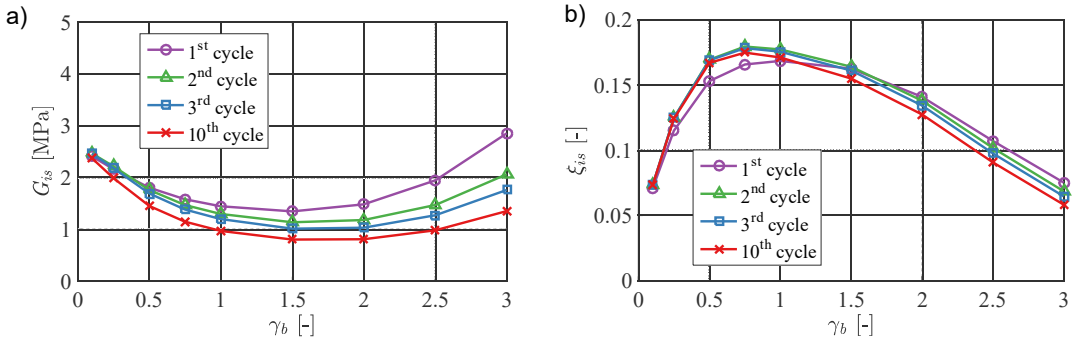

Figure 2: Equivalent linear parameters at different strain amplitudes and cycles: (a) equivalent shear modulus and (b) equivalent damping ratio

In particular, Figure 2a reports values of the secant shear modulus (G_{is}), whereas Figure 2b reports the values of the equivalent damping ratio (ξ_{is}), defined according to (EN15129) by the following expressions, where W_D is the energy dissipated in each cycle:

$$G_{is} = \frac{\tau_{b,\max} - \tau_{b,\min}}{\gamma_{b,\max} - \gamma_{b,\mathrm{mn}}} \tag{1a}$$

$$\xi_{is} = \frac{2W_D}{\pi G_{is}\left(\gamma_{b,\max} - \gamma_{b,\min}\right)^2} \tag{1b}$$

Case study design

The case study considered in this paper consists in a 6-storey three-dimensional reinforced concrete building frame (Figure 3). The beams and columns have a rectangular transverse cross section with height of 500 mm and width of 300 mm. The floors are assumed rigid in plane and have a mass of 200kNms^{-1}. A hybrid isolation system, consisting of 6 HDNR bearings and 9 low friction flat sliders providing mainly a vertical support (Figure 3), is considered. The design of the isolators is carried out by assuming the superstructure as rigid and by considering a target period of vibration $T_{is,d}$=2.5 s. Zero friction of the sliders is assumed for the same design.

The isolation system is dimensioned to attain under the design seismic action a value of the shear deformation equal to $\gamma_{b,d}$ = 1.5, corresponding to a value of the equivalent shear modulus close to the minimum (Figure 2a), and to a value of the equivalent damping ratio close to the maximum (Figure 2b). Thus, the value of $\gamma_{b,d}$ is close to optimal and it is lower than the limit of 2.5/γ_x imposed by the European code on anti-seismic devices (EN1998-1), where γ_x is equal to 1.2 and is the reliability factor prescribed by the same code.

According to European code (EN1998-1), a design action corresponding to the Ultimate Limit State (ULS) of the Eurocode 8 has been considered, characterized by an exceedance probability of 10% in 50 years or a return period T_R=475 year. In particular, a Type 1 spectrum with a peak ground acceleration on stiff soil of 0.35g and soil C conditions are considered for the ULS seismic action. The corresponding peak ground acceleration at the building site is equal to a_g = 0.35g·1.15= 0.403g. Moreover, following the indications given by the EN15129, the design of the isolation system has been carried out by considering nominal values of the equivalent linear properties calculated at the third cycle of imposed cyclic deformations carried out at the selected design shear strain and design period. For the considered rubber compound, the design equivalent shear modulus and the design equivalent damping ratio are respectively $G_{is,d}$=1 MPa and $\xi_{is,d}$=16%. By considering the superstructure as infinitely rigid, and lumping the total mass M over the isolation system, the structure reduces to a S-DOF system and the isolation system displacement can be estimated from the displacement spectrum corresponding to the target isolation period ($T_{is,d}$=2.5s) and the damping ratio of the isolation system ($\xi_{is,d}$ =16%). The obtained displacement is $u_{b,d}$ = 0.207 m, and the total rubber thickness is t_r= $u_{b,d}$ / $\gamma_{b,d}$ =0.138 m. Consequently, the total rubber area (A_{is}) can be obtained through the following expression:

$$A_{is} = \left(\frac{2\pi}{T_{is,d}}\right)^2 \frac{t_r}{G_{is,d}} M \tag{2}$$

The obtained value for unit total mass is A_{is}=0.00086 m^2, which leads to 6 HNDR bearings with diameter D_{is}=504 mm and total rubber thickness equal to t_r=138mm. The secondary shape factor S_2=D/t_r is equal to 3.6. The bearings are obtained by combining 20 rubber layers of thickness t_s=6.9 mm and the primary shape factor S_1=D/4t_s is 18.3. By this way, bearings agree with indications about primary and secondary shape factors given by the standard for buildings isolation (BS ISO 22762-3). The buckling load capacity of the bearings at the design displacement P'_{cr}, calculated according to the theory of the stability of multi-layered rubber compression springs under large lateral displacements (Kelly and Konstantinidis 2011), is equal to 5400 kN, whereas the axial forces due to vertical loads are about 830 kN and 440 kN for central and lateral bearings respectively. It is noteworthy that choice of employing this hybrid isolation system yields large isolators with an ample margin with respect to the buckling load capacity, such that the horizontal behaviour is not influenced by axial loads even under rare seismic events.

In order to verify the outcomes of the design, an equivalent Linear Visco-Elastic (LVE) model of the isolation bearings at the design shear strain ($\gamma_{b,d}$) can be defined, with stiffness $k_{is,d}$ and damping constant $c_{is,d}$, evaluated as follows:

$$k_{is,d} = \frac{G_{is.d} A_{is}}{h_{is} n_{is}} \tag{3a}$$

$$c_{is,d} = \frac{2\xi_{is,d}}{\omega_{is,d}} k_{is,d} = \frac{\xi_{is,d} T_{is,d}}{\pi} k_{is,d} \tag{3b}$$

where n_{is} is the number of bearings adopted (6 in this case study). By adopting the linear model of bearings the complex modal analysis can be carried out on the linear finite element model of the M-DOF system. The model of the system is built by considering a Young modulus of concrete equal to 32000 MPa and a cracking reduction coefficient equal to 0.5 for the beams and 0.7 for the columns of the superstructure. Moreover, as for the 2-DOF systems, a stiffness proportional damping is assumed. The mass-proportional component is set equal to zero because it would lead to underestimate the isolated system response (Ryan and Polanco 2008). The damping constant for the stiffness-proportional damping matrix is calibrated to provide a damping ratio equal to 2% in correspondence of the first vibration period of the fixed-base superstructure. Figure 4 illustrates the absolute values of the undamped eignenmodes of the first three vibration modes of the isolated MDOF system at the design conditions ($\gamma_{b,d}$=1.5, 3rd cycle of imposed deformation history). The relevant mass participation ratios are 0.995, 0.004 and 0.0002 respectively. The vibration period of the two significant modes (the first two modes) are T_1=2.65 s and T_2= 0.55 s. the associated damping ratios are ξ_1=13.4% and ξ_2=10.1%. .As expected the difference be-tween the target isolation period and the actual first period T_1, due to the influence of the superstructure flexibility, is not very significant.

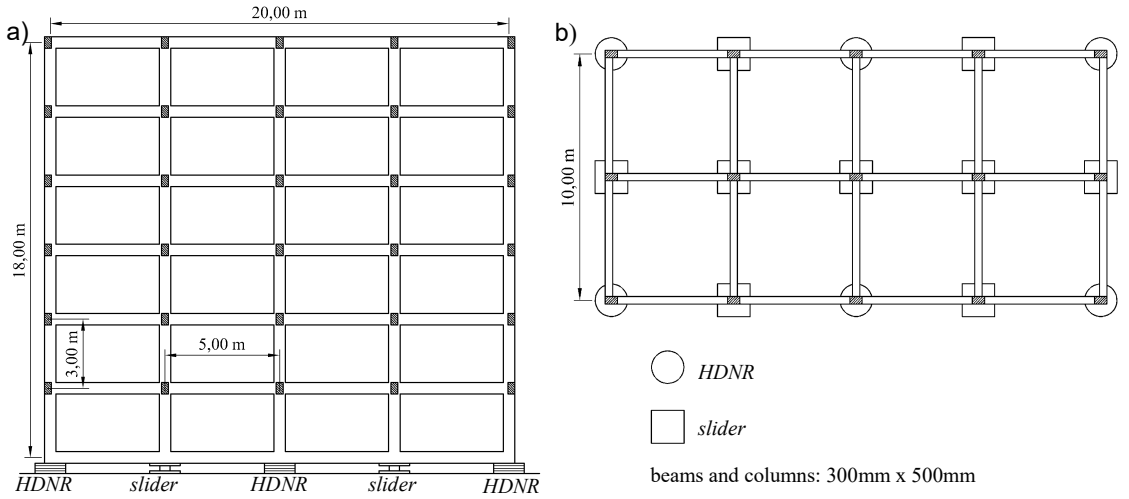

Figure 3: (a) 6-storeys isolated building, and (b) isolation system configuration

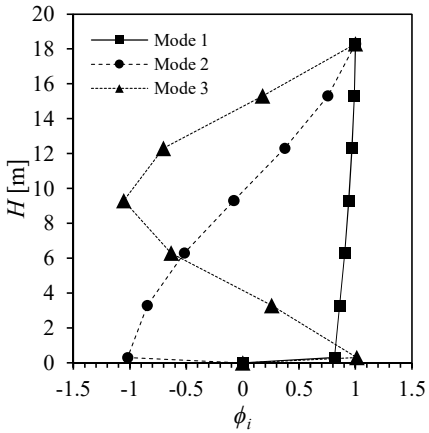

Figure 4: First three modal shapes of the isolated MDOF system for the LVE bearing model

Seismic analyses

Seismic input

A set of 20 ground motion records are employed in the parametric study to describe the record-to-record variability effects. These records have been selected from the PEER strong motion database (Ancheta et al. 2014) based on the following criteria: they are associated to the site class C as defined in Eurocode 8 (EN1998-1), have a source-to-site distance R varying in the range between 20 km and 50 km (thus records do not contain any pulse) and a moment magnitude Mw varying in the range between 6.5 and 7.5. Records are scaled in amplitude to match the ULS spectrum at the design isolation period and damping ratio. Among all the records available for the selected scenario, the 20 selected ones are characterized by scale factors close to 1. Record details and scale factors are reported in Table 1, whereas the response spectra of the scaled records are plotted in Figure 5 together with the average and the design spectrum.

In order to describe the seismic scenario at lower seismic hazard levels, the same ground motions have been further scaled by a factor given by the ratio between the spectral ordinate at the considered limit state and at the design limit state, corresponding to the design isolation period and damping. The values of the peak ground acceleration (a_g) at return periods other than the design one are obtained by considering the following hazard curve for the:

No.	Year	Earthquake Name	Station Name	PGA	V_{s30}	Comp.	M.	R_{rup}	SF
-	-	-	-	[g]	[m/sec]	-	-	[km]	-
1	1995	Kobe_ Japan	Morigawachi	0.17	256	1	6.9	24.8	1.18
2	1995	Kobe_ Japan	Sakai	0.15	256	1	6.9	28.1	1.44
3	1995	Kobe_ Japan	Yae	0.15	256	1	6.9	27.8	1.26
4	1979	Imperial Valley-06	Delta	0.26	242	1	6.5	22.0	1.42
5	1979	Imperial Valley-06	Delta	0.26	242	2	6.5	22.0	1.12
6	1954	Northern Calif-03	Ferndale City Hall	0.19	219	1	6.5	27.0	1.23
7	1968	Borrego Mtn	El Centro Array #9	0.09	213	1	6.6	45.7	1.57
8	1992	Landers	Indio - Jackson Road	0.23	292	1	7.3	48.8	1.21
9	2004	Niigata_ Japan	NIG018	0.13	198	1	6.6	25.8	0.97
10	1989	Loma Prieta	Agnews State Hospital	0.16	240	2	6.9	24.6	0.83
11	1989	Loma Prieta	Hollister - South & Pine	0.29	282	1	6.9	27.9	0.82
12	1989	Loma Prieta	Hollister - South & Pine	0.29	282	2	6.9	27.9	1.54
13	1989	Loma Prieta	Hollister City Hall	0.23	199	1	6.9	27.6	1.40
14	1989	Loma Prieta	Hollister City Hall	0.23	199	2	6.9	27.6	0.96
15	1989	Loma Prieta	Hollister Differential Array	0.28	216	1	6.9	24.8	1.12
16	1989	Loma Prieta	Hollister Differential Array	0.28	216	2	6.9	24.8	1.59
17	1989	Loma Prieta	Sunnyvale - Colton Ave.	0.21	268	1	6.9	24.2	0.82
18	1989	Loma Prieta	Sunnyvale - Colton Ave.	0.21	268	2	6.9	24.2	0.76
19	1992	Cape Mendocino	Eureka - Myrtle & West	0.17	337	2	7.0	42.0	1.34
20	1992	Landers	Palm Springs Airport	0.09	312	2	7.3	36.2	1.29

Table 1: Records details and values of the scale factor (SF) for the design earthquake level

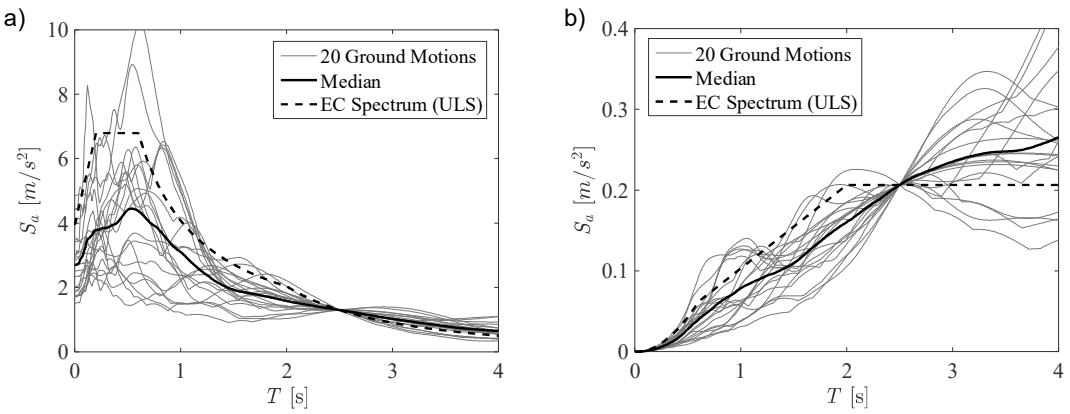

Figure 5: (a) Pseudo-acceleration spectra and (b) displacement spectra of the scaled 20 records, average spectrum and EC8-type 1 design spectrum at ULS for ξis=16%.

$$v\left(a_g\right) = k_0\left(a_g\right)^{-k_1} \tag{10}$$

where k_1 is set equal to 1/0.35=2.857 according to (Lubkowski 2010), and k_0 is set equal to 0.013. The selected parameters provide a peak ground acceleration a_g =0.403g for ν=0.0021 yrs^{-1} (corresponding to T_R=475 yrs), coherently with the design of the isolation system carried out in the previous section. Table 3 reports the values of a_g corresponding to the considered limit states as well as the spectral ordinates in terms of pseudo-acceleration (S_a) calculated at the design isolation period (T_{is}=2.5 s) and for a 5% damping ratio. For completeness, pseudo-acceleration and displacement spectral ordinates calculated by also considering the equivalent damping coefficient of the isolation system (ξ_{is}=16%) are provided in the same table. These are obtained by reducing the spectrum by the factor η=0.7 (EN1998-1). The same spectral shape is assumed for all the return periods.

	T_R	$\nu=1/T_R$	a_g	S_a (T_{is},5%)	S_a(T_{is}, ξ_{is})	S_d (T_{is}, ξ_{is})
	[yrs]	[yrs^{-1}]	[*g*]	[*g*]	[*g*]	[*m*]
OLS	30	0.03333	0.153	0.073	0.051	0.079
DLS	95	0.01052	0.229	0.110	0.076	0.118
ULS	475	0.00210	0.403	0.193	0.133	0.207

Table 2: Limit states and seismic input

Analyses results

This section summarizes the results of the analyses carried out on the base-isolated MDOF system at the design and serviceability limit states. The analyses have been performed by describing the isolation system with the advanced HDNR model accounting for stress-softening developed by some of the authors of this study (Tubaldi et al. 2017 and Ragni et al. 2018) and with two simplified models, defined according to the indications given by design codes (EN1998-1, EN15129). The first simplified model is the LVE model already calibrated at the ULS and introduced for the modal analysis. The second one is the Buoc-Wen (BW) elasto-plastic (EP) model. Both the simplified models have been calibrated for each limit state considering the equivalent damping and stiffness corresponding to the bearings displacements reported in the last column of Table 2. For the LVE model, Eqs. 3a and 3b are considered, whereas for the BW model the following expression has been used to calibrate the characteristic strength at zero strain (τ_0):

$$\tau_0 = \frac{\pi \xi_{eff} G_{eff} \gamma_{b,d}^2}{2\left(\gamma_{b,d} - \gamma_{b,y}\right)} \tag{9}$$

where $\gamma_{b,y}$ is the yield shear strain of the equivalent bilinear model, assumed equal to 0.1, according to (ASCE 41-13). Floor displacements and accelerations estimated using the HDNR, LVE and BW models are depicted in Figure 6 for each limit state in terms of average values. It is evident from the figure that both the simplified models describe with sufficient accuracy the floor displacements. Significant differences are observed only at the ultimate limit state for the LVE model, which seem significantly less stiff or less dissipative compared to the HDNR and BW models. Differently, the floor accelerations are well described only by the BW model, because they are strongly affected by the second vibration mode of the isolated building, whose contribution is well estimated by the advanced HDNR model and the BW model but underestimated by the LVE model.

In Figure 7, the results are reported in terms of median values and 16th and 84th percentiles, for all the limit states and for the three models considered. As expected, compared to the HDNR model, the LVE model shows lower effects of the record-to-record variability for both floor displacements and accelerations, especially at the ULS. This is due to the nonlinear behaviour of the HDNR ant the stress-softening, which makes the HDNR behaviour record-dependent. Differently, the BW model tends to overestimate the variability of the displacements, especially at the ULS. On the contrary, the variability of the floor absolute accelerations is always underestimated, especially at the ULS. These differences are due to the strain hardening and stress-softening of the HDNR model, which are both important at the ULS and neglected by the BW model. In particular, at the ULS, the increasing stiffening of the HDNR model for increasing strains is able to limit the response variation in terms of displacements, but leads to an increased

variability of the floor accelerations, because small variations of displacements cause large variations of isolator forces transmitted to the superstructure.

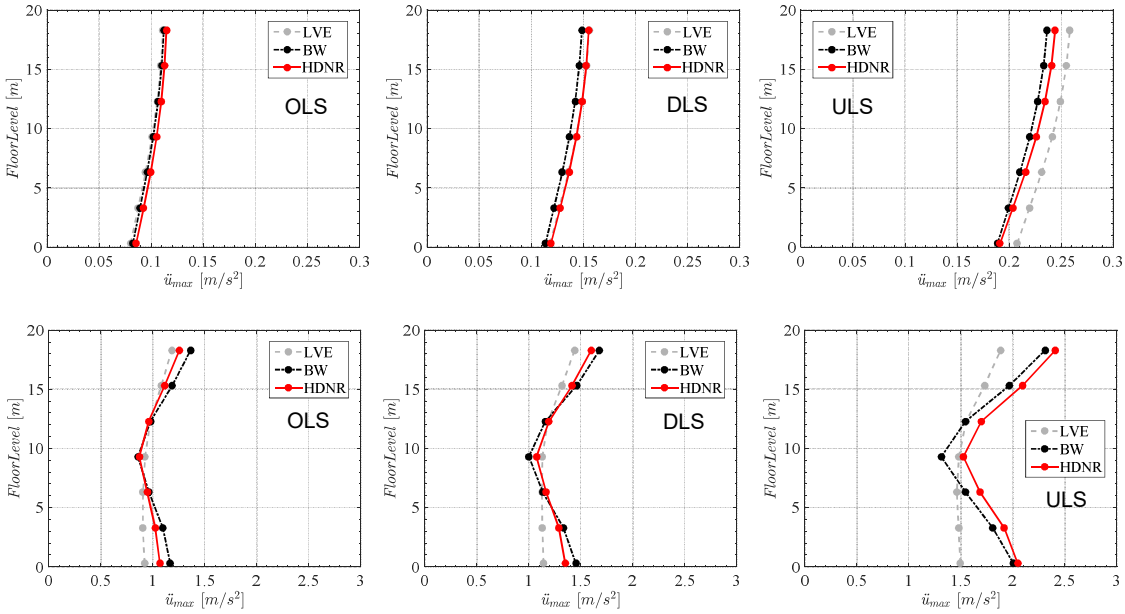

Figure 6: Mean values of (a) maximum displacements and (b) maximum floor accelerations, for the considered intensity levels.

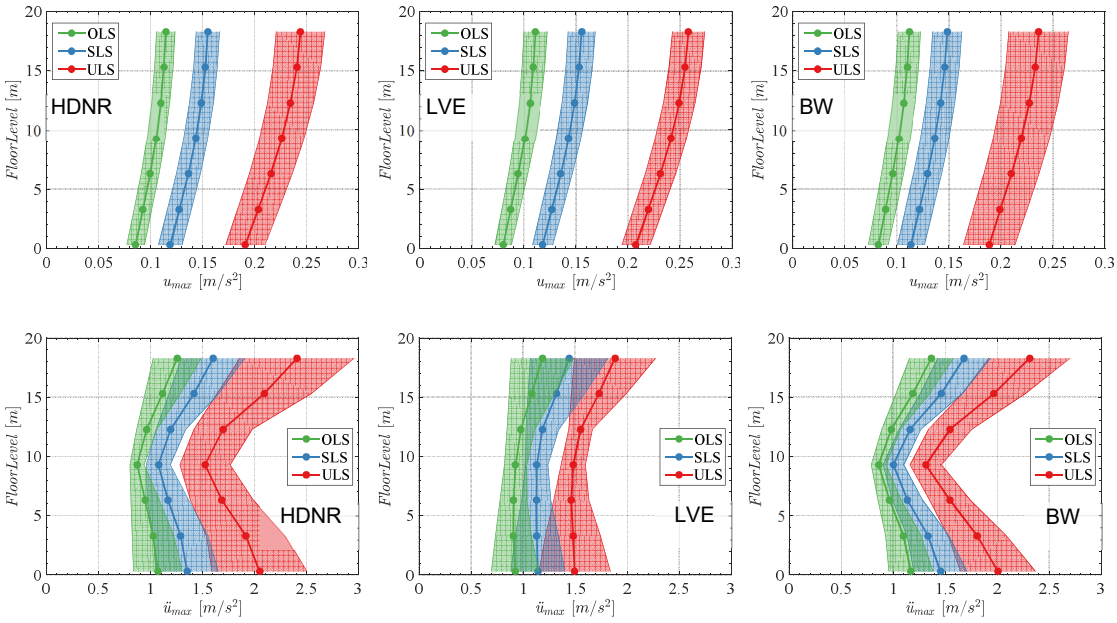

Figure 7: Median values and 16th and 84th percentiles of (a) maximum displacements and (b) maximum floor accelerations, for the considered intensity levels.

In order to evaluate the performance of acceleration-sensitive flexible equipment inside the building, the mean Floor Response Spectra (FRS) under the different records are evaluated for all the building storeys and for all the limit states. Figure 8 illustrates the mean FRS at the OLS, DLS and ULS intensity levels for each floor and for the advanced model and the two simplified models. In all the cases, two major peaks are observed, in correspondence of the first and second vibration period of the isolated system. Moreover, in all the cases the first mode peak slightly increases by passing from the base to the top floor. Differently, in correspondence of the second mode, the peaks of the base and top floors and also of the 1*th* and 5 *th* floors are larger than the peaks of the 2 *th* and 4 *th* floors. This is consistent with the shape of the second mode (Figure 4), resulting in different demands at various floors. For the same reason, the 3rd floor does not exhibit

a peak in correspondence of the second vibration period, since it is located in correspondence of the node of the second modal shape. With reference to the FRS obtained with the HDNR model, it is also observed that peaks in correspondence of the first vibration mode change in shape, value, and location with the seismic intensity level, due to nonlinear and record-dependent behaviour of the isolation system. Moreover, for serviceability limit states (OLS and DLS) the peak in correspondence of the second vibration period is similar in amplitude to the peak in correspondence of the first vibration mode and becomes larger for the design seismic action. With reference to simplified models, the FRS obtained with the LVE models show significantly different trends, whereas these obtained with the BW model are more similar. Figure 9 illustrates the response floor spectrum of the top floor according to the three different bearing models considered. The peaks in correspondence of the first mode obtained with the LVE model are similar or larger in amplitude with respect to those obtained with the HDNR model, but different in shape, especially at the ULS, due to the nonlinear and record-dependent behaviour of the HDNR model. On the contrary, the peaks in correspondence of the second vibration mode obtained with the HDNR model are almost twice those obtained with LVE models, which further confirms that the higher modes response is highly damped by the LVE model. Differently, the FRS obtained with the nonlinear BW model are more similar to those obtained with the HDNR model. In particular, the peaks in correspondence of the first mode are very similar in shapes but a little lower in amplitude, due to the stress-softening effect neglected by this model. On the contrary, the peaks in correspondence of the second vibration mode are overestimated. This is due to the larger stiffness of the BW model for shear strain smaller than the design value, as can be appreciated in Figure 10.

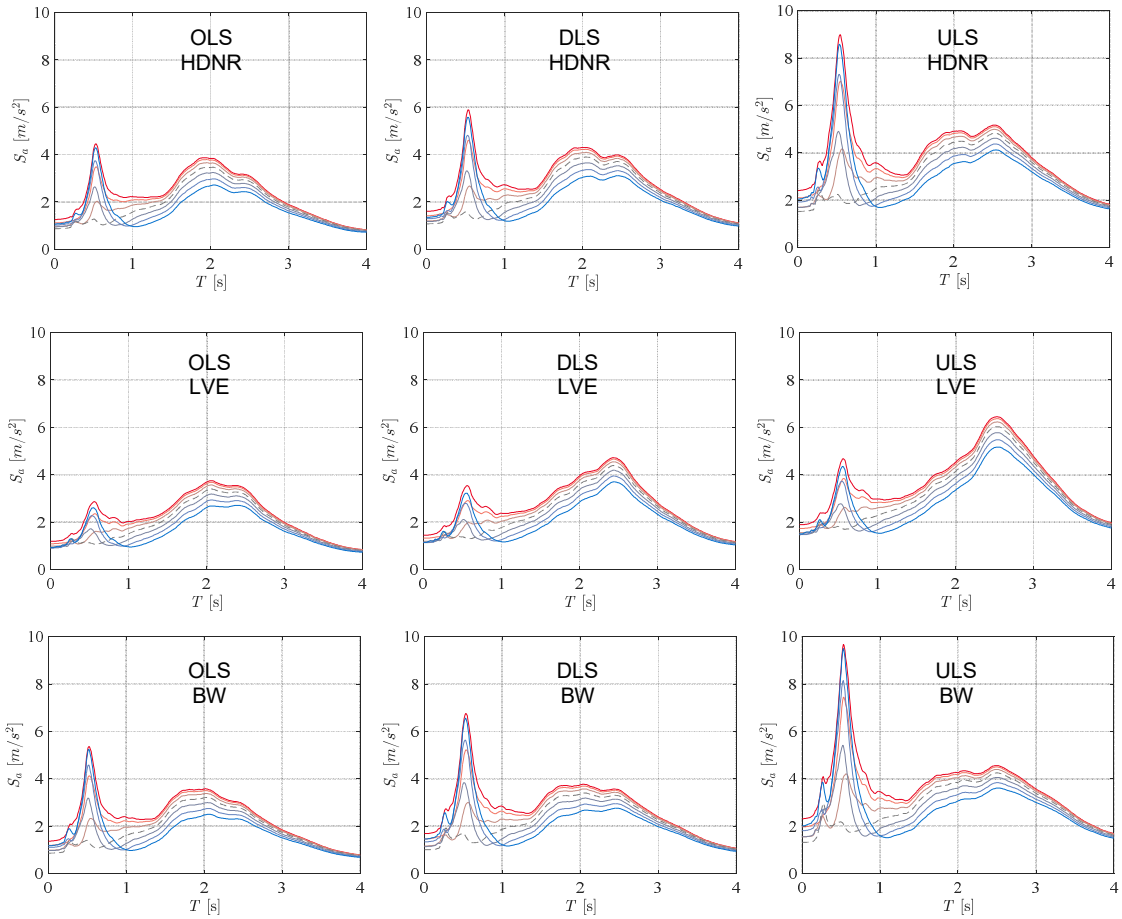

Figure 8: FRS of superstructure floors for different bearing models and intensity levels.

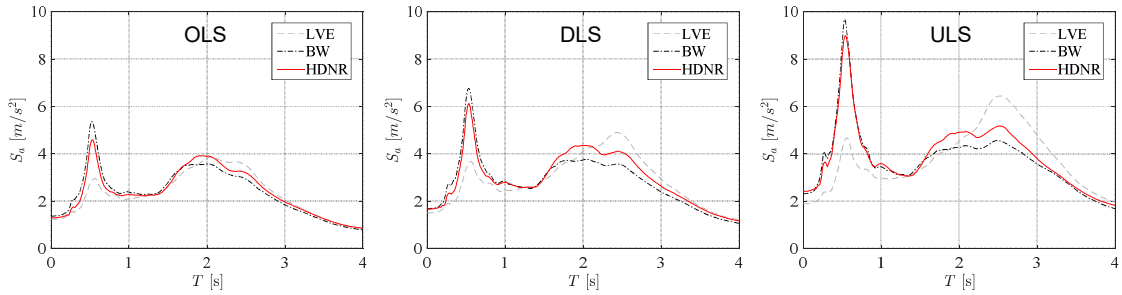

Figure 9: Mean FRS of the top floor at the ULS for different bearing models.

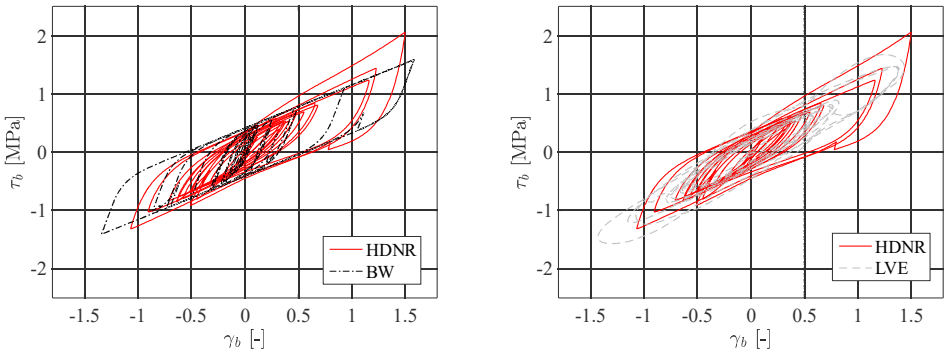

Figure 10: Hysteresis loops under one record scaled to the ULS intensity level for (a) HDNR and BW models and (b) HDNR and LVE models.

CONCLUSIONS

This paper investigates the seismic response of structures isolated by HDNR bearings under increasing seismic intensity levels up to the design one. In particular, the effects of the nonlinear behaviour and the stress-softening are investigated by using a recently-developed advanced HDNR model. The obtained results show that the performance of the superstructure at the serviceability and design limit states is satisfactory, i.e. absolute acceleration and relative displacements of the superstructure do not show excessive amplifications. Moreover, the response estimates obtained with the HDNR bearing model are compared with those obtained with a linear viscoelastic (LVE) and an elasto-plastic (EP) model, both calibrated for each intensity level considered. The comparison shows that in general the EP model provides a good estimate of the base-isolated system response at all the intensity level. Differently, the LVE model overestimates the bearings displacements at the Ultimate Limit State (ULS) level and underestimates the superstructure accelerations at all the intensity level, especially at the lowest and highest floors. This is due to the response contribution of the second vibration mode of the base-isolated system, which is excessively damped by the LVE model. In addition, the LVE model, also notably underestimates the variability of the superstructure and isolation system response, especially at the ULS level. Differently, the EP model tends to overestimate the variability of displacements and to underestimate the variability of the floor absolute accelerations, especially at the ULS level. This is due to the strain hardening and stress-softening of the HDNR model at this limit state, which limit the variability of displacements but increases the variability of the superstructures accelerations. Finally, floor response spectra (FRS) obtained with the HDNR model show peaks in correspondence of the second vibration mode more than two times larger than the corresponding peaks obtained with the LVE model, confirming that the higher modes response is highly damped by the LVE model. The peaks in correspondence of the first mode are more similar in amplitude but different in shape, due to the influence of the nonlinear behaviour and the stress-softening on the dynamic properties of HDNR bearings. Differently, the FRS obtained with the EP model are more similar to those obtained with the HDNR model. In particular, the peaks in correspondence of the first mode are very similar in shapes bur a little lower in amplitude, due to the stress-softening effect neglected by this model, whereas those in correspondence of the second vibration mode are slightly larger.

References

Ancheta TD, Darragh RB, Stewart JP, Seyhan E, Silva WJ, Chiou BSJ (2014), NGA-West2 Database. *Earthquake Spectra,* 30(3): 989–1005.

ASCE 41-13.

BS ISO 22762-3: Elastomeric seismic-protection isolators – Part 3: Applications for buildings – Specification, 2005.

Clark PW, Aiken ID, Kelly JM (1997), Experimental studies of the ultimate behaviour of seismically isolated structures, *Report No. UCB/EERC-97/18*, Earthquake Engineering Research Center, University of California, Berkeley, California.

EN15129. Anti-Seismic devices. European Committee for Standardization, 2018.

EN1998-1. Design of structures for earthquake resistance. European Committee for Standardization, 2013.

Grant DN, Fenves GL, Whittaker AS (2004), Bidirectional modeling of high-damping rubber bearings. *Journal of Earthquake Engineering*, 8(1):161-185.

Isakovic T, Zevnik J, Fischinger M (2011), Floor response spectra in isolated structures subjected to earthquakes weaker than the design earthquake—Part I: Isolation with high-damping rubber bearings, *Struct. Control Health Monit,* 18:635–659

Kelly JM and Konstantinidis D (2011), *Mechanics of Rubber Bearings for Seismic and Vibration Isolation*, John Wiley & Sons, Ltd.

Kelly JM and Marsico MR (2015) The influence of damping on floor spectra in seismic isolated nuclear structures. *Struct. Control Health Monit,* 22:743–756.

Kikuchi M, Nakamura T, Aiken ID (2010), Three-dimensional analysis for square seismic isolation bearings under large shear deformations and high axial loads, *Earthquake Engng Struct. Dyn*; 39:1513–1531.

Lubkowski ZA (2010), Deriving the Seismic Action for Alternative Return Periods According to Eurocode 8, *10th European Conference on Earthquake engineering*, Ohrid.

McKenna F, Fenves G, Scott M. Computer program OpenSees: open system for earthquake engineering simulation, Pacific Earthquake Engineering Center, University of California, Berkeley, CA, 2006.

Mullins L. (1969), Softening of rubber by deformation, *Rubber Chemistry and Technology*, 42(1): 339-362.

NTC 2018. Norme tecniche per le costruzioni. Gazzetta Ufficiale della Repubblica Italiana, 2018.

Ragni L, Tubaldi E, Dall'Asta A, Ahmadi H, Muhr A (2018), Biaxial shear behaviour of HDNR with Mullins effect and deformation-induced anisotropy, *Engineering Structures,* 154: 78-92.

Ryan KL, Polanco J (2008), Problems with Rayleigh Damping in Base-Isolated Buildings, *Journal of Structural Engineering,* 134(11): 1780–1784.

Tubaldi E, Ragni L, Dall'Asta A, Ahmadi H, Muhr A (2017), Stress softening behaviour of HDNR bearings: modelling and influence on the seismic response of isolated structures, *Earthquake Engng Struct. Dyn*, 46(12): 2033-2054.

Yang TY, Konstantinidis D, Kelly JM (2010) The Influence of Isolator Hysteresis on Equipment Performance in Seismic Isolated Buildings, *Earthquake Spectra*, 26(1): 275-293.